END RESONANCES FOR ATOMIC CLOCKS

A. B. Post[(1)], Y-Y. Jau[(1)], N. N. Kuzma[(1)], A. M. Braun[(2)], S. Lipp[(2)], J. H. Abeles[(2)], M. V. Romalis[(1)], E. Miron[(1)], and W. Happer[(1)]
[1] Department of Physics, Princeton University, Princeton, NJ 08544, USA
[2] Sarnoff Corporation, Princeton, NJ 08543, USA

Abstract

We discuss advantages of the "end" resonances for the miniaturized, chip-scale atomic clocks based on alkali-vapor cells filled with high-pressure buffer gases. Compared to the commonly used 0-0 resonance clock design, these advantages include a higher signal-to-noise ratio, a narrower linewidth at high vapor densities, and a significantly reduced sensitivity to the frequency stability of the pump laser at high buffer-gas pressure. We report our measurements of the ^{133}Cs resonance linewidth for both 0-0 and end transitions, and give the estimates of the ^{133}Cs resonance-damping rates due to N_2 buffer gas. Contributions to the total linewidth from other broadening mechanisms are also discussed. Finally, we demonstrate a 1 kHz end resonance linewidth in a MEMS-fabricated microcell containing cesium and 1 atm N_2.

I. INTRODUCTION

The development of miniature atomic clocks **[1,2]** is potentially promising for mobile jam-resistant GPS receivers and high-security UHF communication. For traditional alkali vapor-cell atomic clocks, spin-exchange collisions are the main contribution to the resonance linewidth **[3]**. The spin exchange broadens the linewidth, reduces the signal-to-noise ratio (SNR), and, hence, increases the uncertainty of the traditional clock resonance. The effect of this line-broadening mechanism is more severe in miniature cells, where alkali-vapor density must be increased to obtain an adequate signal from the cell over a much shorter optical-path length.

Clock resonances are based on the hyperfine splitting of stable alkali-metal isotopes, such as ^{133}Cs or ^{87}Rb. The atomic clock cells are filled with an alkali metal and a buffer gas, such as N_2. At a given temperature, some alkali atoms are in a vapor phase. A laser tuned to the D1 line between the *S* ground state and the lowest *P* state of the alkali atom is used to selectively excite the atoms from one of the two ground-state multiplets *F*, where $F=I\pm1/2$ is the total angular momentum of the alkali atom in units of $\hbar$, and *I* is the nuclear spin quantum number. A population imbalance is achieved between the two $I\pm1/2$ hyperfine multiplets. Microwave radiation, tuned to the multiplet-splitting frequency, generates a coherent superposition state, generally between the two field-independent sublevels with the azimuthal angular momentum quantum number $m_F = 0$, shown in Figure 1. This is the traditional 0-0 clock resonance.

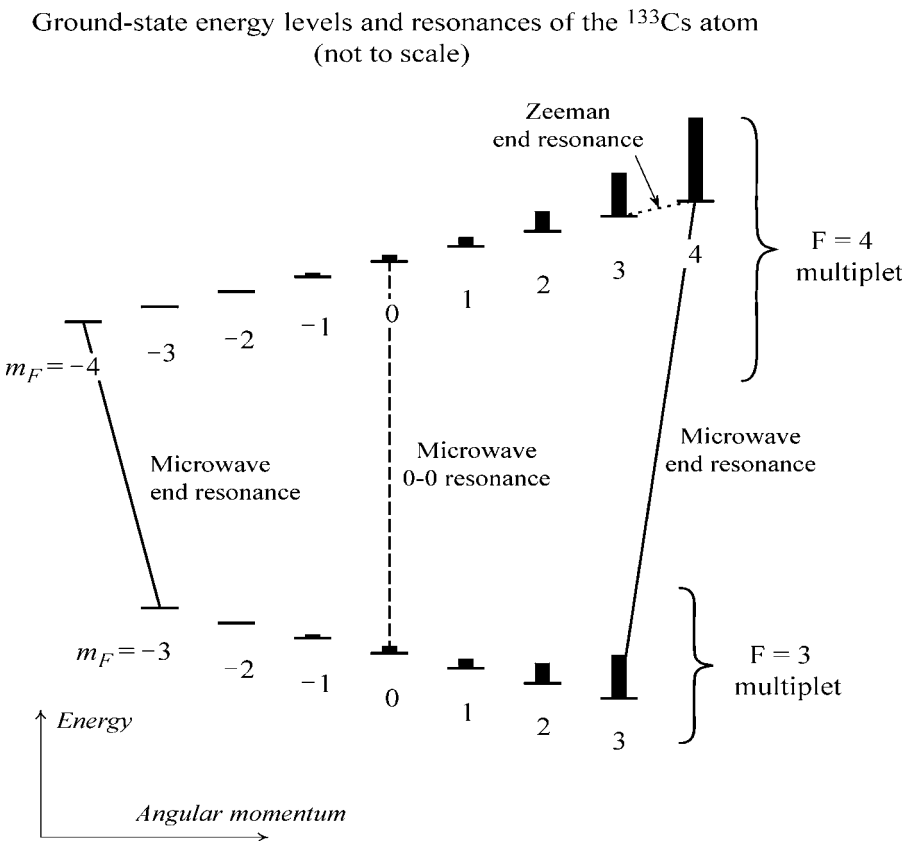

Figure 1. The ground state hyperfine levels of ^{133}Cs with I = 7/2.

The short-term stability of an atomic clock has traditionally been measured by the Allan deviation **[4-6]**

$$\sigma_y \propto \frac{1}{\mathrm{SNR}\cdot Q} = \frac{\Delta\nu}{\mathrm{SNR}\cdot \nu_{\mathrm{hf}}}, \qquad (1)$$

where the oscillator quality factor Q is the ratio of the transition frequency ν_{hf} to the linewidth $\Delta\nu$. The high density of the alkali-metal vapor needed to compensate for the small cell size broadens the linewidth and decreases the signal-to-noise ratio of the 0-0 resonance. Hence, both the numerator and denominator of Eq. (1) are degraded in miniature clocks. Because spin-exchange collisions conserve the total spin of the colliding pair of alkali-metal atoms, the end resonances are much more suitable for high-temperature operation. For the traditional 0-0 resonance, the colliding atoms have zero time-averaged spin. There are $2(2I+1)$ final states to which the collisions can transfer the atoms, so spin-exchange collisions effectively interrupt the coherent oscillation and broaden the width of this transition. In addition, the atoms are nearly equally distributed among all possible ground-state hyperfine levels shown in Figure 1 and, thus, only a small fraction of them participates in 0-0 resonance. On the other hand, colliding atoms in the end spin states have maximum (or minimum) spin angular momentum. Pumping with circularly polarized D1 light places most of the atoms in the high-spin states needed for the end resonances, ensuring that nearly all of the atoms participate. This effect substantially increases the signal-to-noise ratio of the end resonance transition. There is no simple way to pump all of the atoms into the two sublevels needed for the traditional 0-0 resonance, so only a small fraction of the atoms can participate. The broadening of the end resonance transitions caused by spin-exchange collisions is also relatively small, as there is just one

final state of the same high angular momentum, e. g. $m_F = I + 1/2 = 4$, to which the colliding Cs atoms can be transferred.

The 0-0 resonance has a second-order frequency-shift dependence on the ambient magnetic field. The coefficient of this shift is small enough that it is possible to operate 0-0 clocks with modest control of the magnetic field. However, the end resonance has a frequency shift directly proportional to the magnetic field, and the coefficient of the shift is large enough that active control of the field is necessary. By locking the local oscillator frequency and the magnetic field to both the microwave and Zeeman end resonances, it is possible to obtain adequate clock stability.

In the following sections, we report experiments that demonstrate narrow linewidths and high SNR of the end resonances. We present data validating the superior signal-to-noise of end resonances in ^{133}Cs compared to the 0-0 resonance.

II. RESONANCE LINEWIDTH CONTRIBUTIONS

There are five dominant contributions to the linewidth: (I) Optical pumping **[7]** of the Rb atoms with a photon flux Φ and a photon absorption cross section σ adds a contribution of order $\sigma\Phi$. (II) Spin-exchange collisions **[8, 9]** between pairs of Rb atoms of number density [Rb] make a contribution **[3]** to the linewidth on the order of the spin-exchange rate. (III) Spin-rotation interactions **[7,10]** during collisions with nitrogen molecules of number density $[N_2]$ contribute to the linewidth on the order of the S-damping rate $\kappa_{sd}[N_2]$. (IV) The modification of the hyperfine splitting **[11-13]** during collisions with the nitrogen molecules makes a contribution to the linewidth on the order of the Carver rate $\kappa_C[N_2]$. Recent experimental measurements of the rate coefficients κ_{ex} , κ_{sd} , and κ_C can be found in **[12,14]**. (V) The final contribution is $D_0(l^2[N_2])^{-1}$, the spin-diffusion rate **[15]**, which determines how fast the atoms relax on the cell walls. Increasing the buffer gas density $[N_2]$ diminishes the linewidth contribution from diffusion to the cell walls, but increases the collisional contribution from the spin-rotation and hyperfine pressure-shift interactions. Simultaneously, increasing the buffer gas density $[N_2]$, corresponding to the buffer gas pressure $p(N_2)$, broadens the optical absorption spectrum, as shown in Figure 2.

This broadening destroys the 0-0 resonance contrast, but does not affect the end transitions. The broad optical absorption spectrum is, in fact, an advantage to practical clock operation based on the end transitions, because it reduces clock's sensitivity to laser frequency fluctuations and diminishes the resonance frequency shifts due to finite light intensity at the cell.

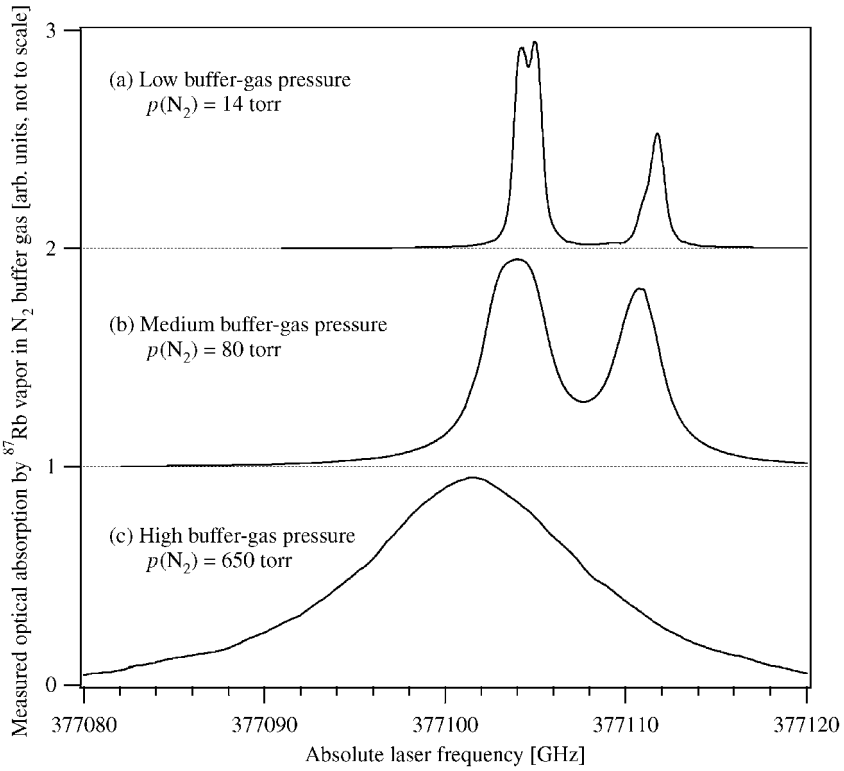

Figure 2. The ^{87}Rb optical absorption spectra demonstrate the broadening and eventual disappearance of the hyperfine structure as the N_2 buffer-gas pressure approaches 1 atm. The optical absorption scans were performed at the cell temperatures of (a) 70°C, (b) 85°C, and (c) 60°C; using (a) 1.5, (b) 0.8, and (c) 3.6 mW/cm^2 of linearly-polarized laser light.

III. EXPERIMENTAL PROCEDURE AND METHODS

The experimental setup is shown in Figure 3. The cell is mounted inside an air-heated non-conductive oven, controlled by a temperature-sensor feedback loop. The laser beam is generated by a *Toptica* external-cavity diode laser system. The laser intensity is attenuated using neutral density (ND) filters, and the circular polarization is achieved using a polarizing beam splitter and a quarter-wave plate. The cell is irradiated by the microwaves emitted from a horn antenna, placed outside of the oven. The microwaves are switched on and off at a low frequency of 50 Hz to facilitate the detection of resonances. There are three sets of Helmholtz coil pairs for compensating the ambient magnetic field and its gradients, and one set for producing the 4.5-gauss B_z field.

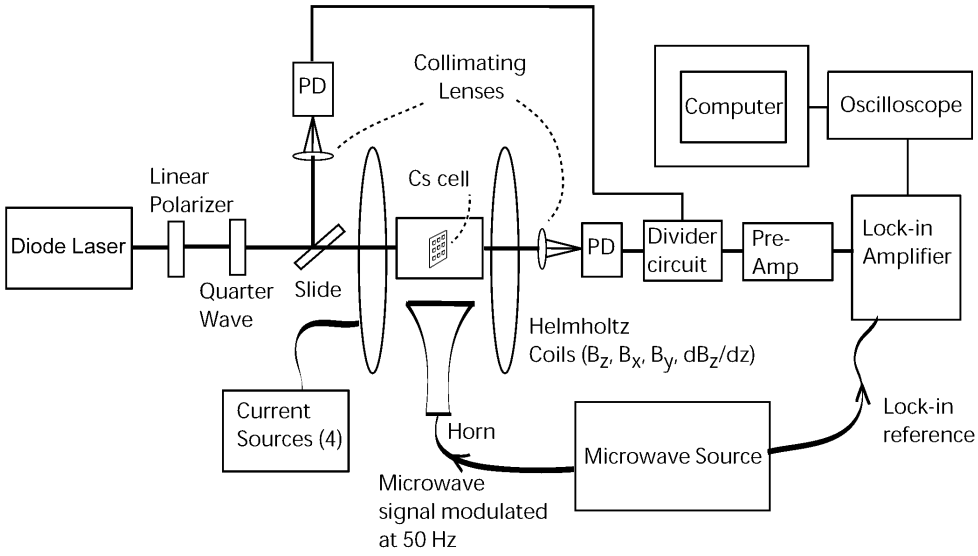

Figure 3. Experimental apparatus.

Two methods have been used to determine the linewidth: the frequency scanning method and the transient method. The frequency scanning method is simple: the microwave frequency is swept through the resonance and the photodetector signal is fed into a lock-in amplifier, tuned to the 50-Hz microwave switching frequency to reduce the noise of the detected optical signal. The transient method is based on detecting the transient response of the atoms to the onset of the microwave radiation. When the microwaves are switched on, the light signal shows an oscillating decay as the atoms coherently precess about the sum of the static field and the oscillating magnetic field of the microwaves. The oscillation frequency of the transient is approximately that of the microwave detuning frequency, which is the difference between the resonance frequency of the atom and the frequency of the microwaves. After the oscillations become sufficiently damped, the photodetector signal decays to a lower, constant value. For the relatively large detunings used in this work, simple theory predicts that identical widths should be obtained for scanned resonances, extrapolated to zero microwave power. We have experimentally verified this predicted equality of the widths obtained by the two methods. The transient method has the advantages that the signal power is centered at many kHz, reducing the problem of $1/f$ noise associated with simple frequency scans. The transient method is also preferred, because its linewidth is not broadened by the microwave power. These advantages result in relatively rapid data acquisition times, making the transient method our preferred technique for efficient studies of the linewidths. For the actual clock implementation, CPT methods **[16-19]** will be utilized.

IV. EXPERIMENTAL RESULTS

The data in Figure 4 show the striking difference observed experimentally between the two resonances in Cs: the linewidths are comparable, but the end resonance has a much better SNR, about 60, compared to its 0-0 counterpart, which exhibits an SNR of only about 2. The two frequency scans were performed at the same experimental conditions: temperature, laser power, and microwave power. At high temperatures, the spin-exchange rate dominates the linewidth unless there are no allowed states to exchange with, as is the case for the end resonance at a high spin polarization.

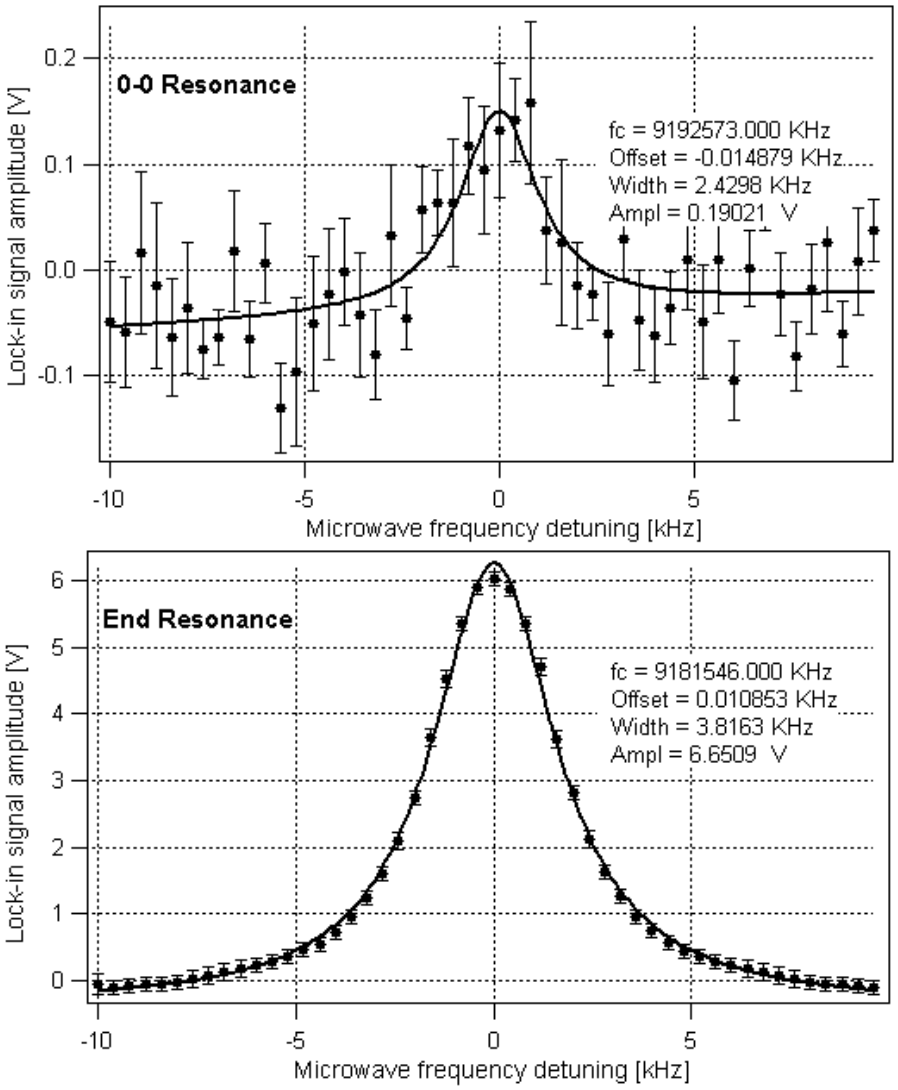

Figure 4. Two microwave-resonance frequency scans at 80 ^{0}C from a hand-made 1mm-thick Pyrex cell filled with Cs and 0.5 atm of N_2. Under the same microwave power and laser intensity, the 0-0 resonance (top panel) has an SNR of only about 2. The SNR of the end resonance (bottom panel) is about 60.

V. DAMPING RATES FOR ^{87}RB AND ^{133}CS

Careful measurements were performed earlier **[14]** to determine the broadening of the Rb linewidth due to the buffer gas pressure. The damping rate was determined to be $\Delta\nu$ = 272 ± 16 Hz amg^{-1}. The measurement of the Carver rate contribution to the Cs linewidth is underway. The dependence of Cs damping rates on buffer-gas density can be estimated, based on our understanding of these rates in Rb. The Carver rate for Rb, reported by Walter *et al.* **[12]**, is

$$\frac{\Gamma_C(\mathrm{Rb})}{[N_2]} = 395 \pm 62 \text{ amg}^{-1}\text{s}^{-1}. \qquad (2)$$

The Carver rate is proportional to $(I(\partial \nu_{hf}/\partial p)_T/\mu_I[I])^2$, where $(\partial \nu_{hf}/\partial p)_T$ is the known pressure-shift coefficient, μ_I is the nuclear magnetic moment, and $[I] = 2I + 1$. Using the calculated pressure shifts, μ_I, and I for Cs and Rb, we expect for the Carver rate of Cs to be 3.1222 Γ_C(Rb). The contribution of the Carver rate to the microwave linewidths is

$$\frac{\Delta\nu}{[\mathrm{N}_2]} = \frac{\mu_I^2[I]^2}{32\pi(\mu_N I)^2}\Gamma_C, \tag{3}$$

where μ_N is the nuclear magneton. We estimate that the contribution of the Carver rate to the microwave resonance in cesium will be about $\Delta\nu$ = 426 Hz amg^{-1}.

VI. PREPARATION OF CS BATCH-FABRICATED MICROCELLS

Alkali cells of 10-mm^3 volume (~3.1 mm x 3.1 mm x 1 mm) were fabricated within a Pyrex/silicon/Pyrex wafer structure. The cells were assembled from two layers of Pyrex glass anodically bonded to an etched silicon central layer; 2" square Pyrex sheet glass (635 μm thick) was utilized.

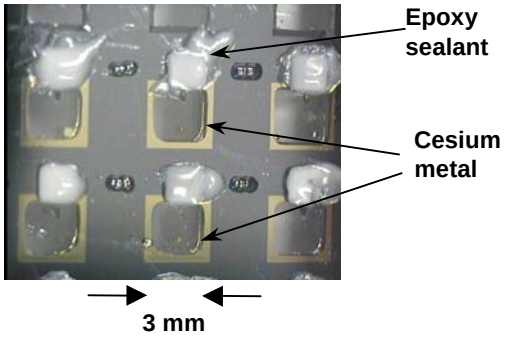

Figure 5. Complete array of 1-mm thick etched cesium microcells. Silicon, anodically bonded to polished pyrex plates, forms 10-mm^3 alkali-vapor microcells. Cesium fill was performed in a heated glovebox backfilled with N_2 at a pressure of 1.5 psi (~ 80 torr) above atmospheric.

A 1-mm thick 4" silicon wafer was patterned/etched to provide the 1 mm optical path-length cells. The silicon wafer was coated on both sides with silicon nitride and photolithographically patterned using a mask containing 3.5 mm square apertures. This pattern was aligned on both sides of the wafer. Windows 3.5 mm on a side were opened in the silicon nitride, and the patterned (1,0,0) Si was subsequently etched through from both sides using a KOH-based solution. This etchant results in a minimum opening in the silicon mid-plane of dimensions 2.8 mm x 2.8 mm. Following removal of the silicon nitride, the Si wafer was anodically bonded to a 2" square, unpatterned, polished Pyrex glass plate.

On the second polished Pyrex plate, 250-μm diameter, oblique-incident, laser-drilled through-holes were made at positions corresponding to the 3.5-mm open cavity. This Pyrex plate was aligned to the Si/Pyrex wafer, and anodically bonded forming the 10-mm^3 cavity. The laser-drilled holes allowed for Cesium fill and seal. The array of cells was then evacuated to remove any residual air and water and subsequently back-filled with nitrogen. The Pyrex/silicon/Pyrex plate was transferred to a glovebox maintained at 35°C and operated with dry nitrogen at 1.5 psi (~ 80 torr) above atmosphere. Cesium metal was drawn

into a syringe tip, which was then inserted through the fill-hole into the cell. The Cs was dispensed into each cell, the needle withdrawn, and the hole sealed with Torrseal™ epoxy. Approximately 0.2 µliter of cesium was dispensed into each cell, preferentially wetting the Si frame of the cell and leaving a clear window needed for optical pumping (see Figure 5). At room temperature, the cells contain 1 atm pressure of N_2 buffer gas. Such wafer-scale processing allows for approximately one hundred 10-mm^3 alkali-vapor microcells on a 2" wafer.

VII. 1 KHZ LINEWIDTH IN A MEMS-FABRICATED CS CELL

With sufficiently low laser power and temperature, a sub-kilohertz linewidth can be observed in Cs using the transient method, which is not affected by the microwave power broadening. After sufficient reduction of both the temperature and laser intensity, it is possible to observe linewidths below 1 kHz. The transient signal for a MEMS-fabricated microcell at 60 °C and 1 mW/cm^2 is shown in Figure 6.

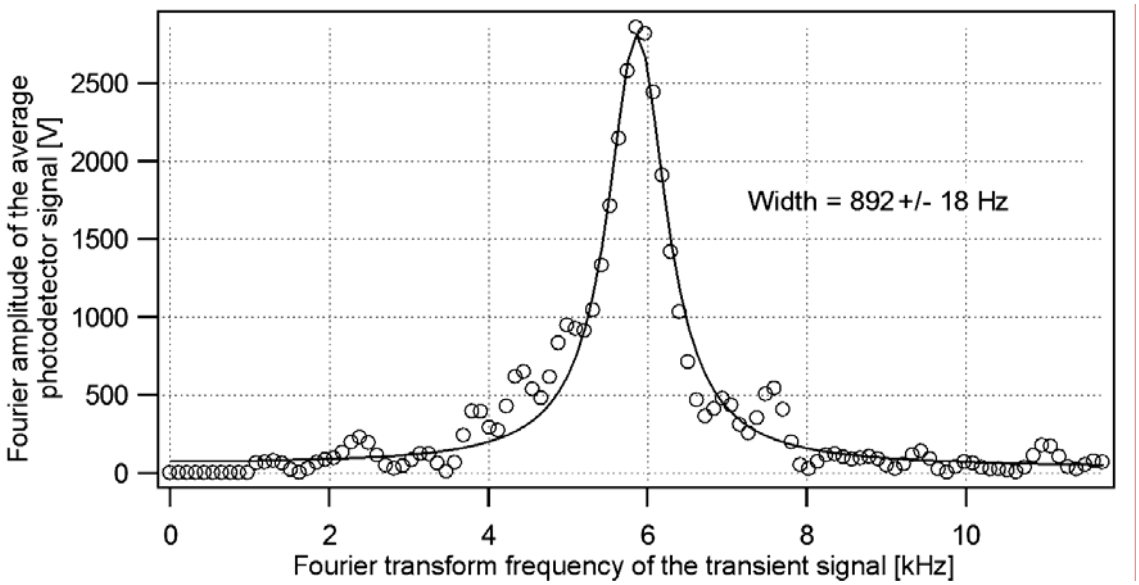

Figure 6. The Fourier transform of a transient signal from a MEMS-fabricated Cs microcell at 60°C shows a linewidth under 1 kHz.

VIII. CONCLUSIONS AND FURTHER WORK

This paper has summarized advantages of considering the end resonances at high buffer-gas pressure for a chip-scale atomic clock time-base, instead of the traditional 0-0 resonances. We have no reports of long-term stability or accuracy, as we have yet to construct a functional clock in our laboratory. The reported experimental results are based on a resonance signal excited by an external microwave source. We will proceed to detect the resonance signal by using an intensity modulated laser beam to both excite and probe the resonance. The advantages of using the end resonance in such system are expected to be the same as those reported here.

IX. ACKNOWLEDGMENTS

We are grateful to many people for their help in this work. We are especially thankful to Michael Souza at the Chemistry Department of Princeton University, who made the cells used in the measurements reported in Figure 4. We are also thankful to Prof. Jacques Vanier for insightful discussions and to Brian Patton for maintaining the high-vacuum cell-filling station. This work was supported by the Defense Advanced Research Projects Agency (DARPA) and the Air Force Office of Scientific Research (AFOSR).

Part of the research reported in this publication was performed by the Sarnoff Corporation in connection with contract/instrument NBCHC020045 with the Department of the Interior. The views and conclusions contained in this publication are those of the authors and should not be interpreted as presenting the official policies or position, either expressed or implied, of the Department of the Interior, or the U.S. Government unless so designated by other authorized documents. Citation of manufacturer's or trade names does not constitute an official endorsement or approval of the use thereof. The U.S. Government is authorized to reproduce and distribute reprints for government purposes notwithstanding any copyright notation hereon.

REFERENCES

[1] J. Kitching, L. Hollberg, S. Knappe, and R. Wynands, 2001, "*Compact atomic clock based on coherent population trapping,"* **Electronics Letters, 37,** 1449-1451.

[2] R. Lutwak, D. Emmons, W. Riley, and R. M. Garvey, 2003, "*The chip-scale atomic clock: Coherent population trapping vs. conventional interrogation,"* in Proceedings of the 34th Annual Precise Time and Time Interval (PTTI) Systems and Applications Meeting, 3-5 December 2002, Reston, Virginia, USA (U.S. Naval Observatory, Washington, D.C.), pp. 539-550, *http://tycho.usno.navy.mil/ptti/ptti2002/paper52.pdf*.

[3] D. K. Walter and W. Happer, 2002, "*Spin-Exchange Broadening of Atomic Clock Resonances,"* **Laser Physics, 12,** 1182-1187.

[4] R. F. Lacey, A. L. Helgesson, and J. H. Holloway, 1966, "*Short-Term Stability of Passive Atomic Frequency Standards,"* **Proceedings of the IEEE,** 170-176.

[5] D. W. Allan, 1987, "*Time and Frequency (Time-Domain) Characterization, Estimation, and Prediction of Precision Clocks and Oscillators,"* **IEEE Transactions on Ultrasonics, Ferroelectrics, and Frequency Control, UFFC-34,** 647-654.

[6] L. Maleki, 2000, "*Tutorial on Advanced Atomic Clocks"* in the 2000 IEEE International Frequency Control Symposium, 6-9 June 2000, Kansas City, Missouri, USA (IEEE Publication 00CH37052), *http://www.ieee-uffc.org/ freqcontrol/tutorials /FCS%20Tutorials%2000/Maleki_files/frame.htm*

[7] S. Appelt, A. B.-A. Baranga, C. J. Erickson, M. V. Romalis, A. R. Young, and W. Happer, 1998, "*Theory of spin-exchange optical pumping of ^{3}He and ^{129}Xe,"* **Physical Review A, 58,** 1412-1439.

[8] L. C. Balling, F. M. Pipkin, and R. J. Hanson, 1964, "*Frequency Shifts in Spin-Exchange Optical Pumping Experiments,"* **Physical Review, 133,** A607-A626.

[9] F. Grossetête, 1964, "*Relaxation par collisions d'échange de spins,"* **Journal de Physique, 25,** 383-396.

[10] R. A. Bernheim, 1962, "*Spin Relaxation in Optical Pumping,"* **Journal of Chemical Physics, 36,** 135.

[11] H. Margenau, P. Fontana, and L. Klein, 1959, "*Frequency Shifts in Hyperfine Splitting of Alkalis Caused by Foreign Gases,"* **Physical Review, 115,** 87-92.

[12] D. K. Walter, W. M. Griffith, and W. Happer, 2002, "*Magnetic slowing down of spin relaxation due to binary collisions of alkali-metal atoms with buffer-gas atoms,"* **Physical Review Letters, 88,** art. no. 093004.

[13] P. J. Oreto, Y.-Y. Jau, A. B. Post, N. N. Kuzma, and W. Happer, 2004, "*Buffer-gas-induced shift and broadening of hyperfine resonances in alkali-metal vapors,"* **Physical Review A,** submitted.

[14] Y.-Y. Jau, A. B. Post, N. N. Kuzma, A. M. Braun, M. V. Romalis, and W. Happer, 2004, "*Intense, Narrow Atomic-Clock Resonances,"* **Physical Review Letters,** submitted.

[15] W. Happer, 1972, "*Optical Pumping,"* **Reviews of Modern Physics, 44,** 169-249.

[16] W. E. Bell and A. L. Bloom, 1961, "*Optically Driven Spin Precession,"* **Physical Review Letters, 6,** 280-281.

[17] G. Alzetta, A. Gozzini, L. Moi, and G. Orriols, 1976, "*Experimental Method for Observation of Rf Transitions and Laser Beat Resonances in Oriented Na Vapor,"* **Nuovo Cimento B, 36,** 5-20.

[18] N. Cyr, M. Tetu, and M. Breton, 1993, "*All-Optical Microwave Frequency Standard – a Proposal,"* **IEEE Transactions on Instrumentation and Measurement, IM-42,** 640-649.

[19] A. Godone, F. Levi, and J. Vanier, 1999, "*Coherent microwave emission without population inversion: A new atomic frequency standard,"* **IEEE Transactions on Instrumentation and Measurement, IM-48,** 504-507.

QUESTIONS AND ANSWERS

GAETANO MILETI (Observatoire de Neuchâtel): I have a question on your comparison of the 0-0 transition signal to noise to the nth transition. In your experiment, I suppose you have used sigma plus polarized light?

AMBER POST: We used sigma plus polarized light for the end resonances, but not for the 0-0 resonances. We don't want to trap them in that state. But, for 0-0, you just want to depopulate one of the hyperfine levels.

MARC WEISS (National Institute of Standards and Technology): Maybe I missed it, but how do you plan to compensate for the magnetic sensitivity of this?

POST: Right, that is a good question. You didn't miss it. We haven't really gotten a good slide on this yet. What we have proposed doing in our proposal is that we would also like to simultaneously detect the Zeeman resonance. If we simultaneously detect the Zeeman resonances, that will be the way that we lock the ambient magnetic field. Our final design would be probing the microwave resonances for the clock and the Zeeman resonances for the magnetic field stability.